



## Super-long span bridge aerodynamics: first results of the numerical benchmark tests from Task Group 10

**Ketil Aas-Jakobsen**

*Dr. Ing. A. Aas-Jakobsen AS, Norway*

**Andrew Allsop**

*ARUP, United-Kingdom*

**Igor Kavrakov**

*Bauhaus-University Weimar, Germany*

**Allan Larsen**

*COWI, Denmark*

**Ole Øiseth**

*Norwegian University of Science and Technology, Norway*

**Tommaso Argentini, Giorgio Diana, Simone Omarini, Daniele Rocchi**

*Politecnico di Milano, Italy*

**Martin Svendsen**

*Ramboll, Denmark*

**Guy Larose, Stoyan Stoyanoff**

*RWDI, Canada*

**Ho-Kyung Kim**

*Seoul National University, Korea* **Santiago Hernández**

*University of A Coruna, Spain*

**Teng Wu**

*University of Buffalo, USA*

**Michael Andersen**

*Svend Ole Hansen ApS, Denmark*

**Hiroshi Katsuchi**

*Yokohama National University, Japan*

Contact: [tommaso.argentini@polimi.it](mailto:tommaso.argentini@polimi.it)

### Abstract

The IABSE Task Group 10 (super-long span bridge aerodynamics) has the mandate to create a standard procedure for validation of methodology and software programs applied for stability and buffeting response analyses of super-long span bridges. Precise estimations of structural stability and response to strong winds are critical for the successful design of long-span bridges.

Task Group 10 covers several important problems related to its mandate including: review and verification of methods developed and adopted by researchers and bridge designers; the definition of guidelines and sample tests for verification and calibration of analytical procedures; identification of fundamental problems of the computation methods; relevant input and output data.

Since the beginning of its work, this working group has developed a 3-step benchmark, with multiple sub-steps of fundamental problems to resolve. The first step of this benchmark has been a numerical comparison of the results obtained using different models adopted across the workgroup members. Using the same inputs: flutter stability and the buffeting response of both a

deck sectional model and a full bridge are studied. Step 2 will be the comparison of predicted results and experimental tests in wind tunnels, and Step 3 will be of validation against full scale measurements.

In this paper, the results of Step 1 will be presented, highlighting critical issues and differences found during the comparison of results. The response of a 3-degrees of freedom bridge deck will be presented both in terms of aeroelastic stability and buffeting response. The results presented are intended to be a reference for the validation of methodologies and software programs that solve for wind response of bridges.

**Keywords:** benchmark; aeroelasticity; flutter; buffeting; long-span bridge

## 1 Introduction

### 1.1 Task of the working group

The objective of the Task Group 10 is the definition of a standard procedure for validating the software programs for the solution of the bridge response to the incoming turbulent wind.

For long-span bridges, the control of wind response is one of the major challenges for the designers, since excessive wind-induced vibrations may lead to comfort, fatigue and structural strength problems. Moreover, structural safety verifications must account for various types of divergent instabilities, such as flutter, galloping.

In other fields of engineering, certified software programs are available, as for example:

- a) software for computing the response of High Voltage Transmission lines to vortex induced vibrations and sub-span oscillations: the software is validated through benchmarks between different programs and against field measurements. [Cigre, EPRI]
- b) software for computing train dynamics to support homologation: the European Standard defines the procedure to validate the software, through comparison between analytical and experimental results. [UIC 518, EN 14363]
- c) software for computing pantograph-catenary interaction. A European Standard to certify the software using a reference computation is available. [EN 50318]

For bridges however, up to now there is no well-established or standardized procedure to predict

stability and response to wind, therefore a 3-step benchmark with increasing complexity has been introduced by the TG 10.

Currently, this TG consists of academic researches, consultants and designers with great experience of bridge studies and design, including Aas-Jakobsen, ARUP, Bauhaus University, Bentley, Bouygues, COWI, Greisch, Norwegian University of Science and Technology, Parsons, Politecnico di Milano, Ramboll, RWDI, Seoul National University, Svend Ole Hansen ApS, Tonji University, University of A Coruna, University of Buffalo, University Southern Denmark, and Yokohama National University. Several methodologies are used to solve the bridge response to wind problems, either in time domain (TD) or in frequency domain (FD); the methodologies employed in current analysis can be found in references [1]-[23].

### 1.2 Benchmark

The Step 1 of the benchmark is a numerical comparison of different solution methods, with the same inputs: critical flutter speed and buffeting response of both a sectional model and a full bridge are studied. Step 2 will be the comparison of predicted results and wind tunnel experimental tests, and Step 3 will be of comparisons against full scale measurements.

Step 1 consists of two sub-steps: Step 1.1 in which the numerical response of 2/3 degree-of-freedom (DOF) simple sectional model is considered; Step 1.2 where a full bridge model and a multi-correlated wind field are considered.

In this paper, the first results of Step 1.1 will be presented, highlighting critical issues and the main

differences arisen during the comparison of the results.

The results presented are intended to be a reference for the validation of software programs that solves for wind response of bridges. An extended and complete report with Step 1 results will be issued in the near future.

## 2 Benchmark: Step 1.1

### 2.1 Step 1.1 Cases

Step 1.1 was conceived to analyse cases with increasing complexity:

Case a) 2-DOFs (vertical and torsional) sectional deck model with theoretical aerodynamic coefficients of a flat plate;

Case b) same as Case a), but with experimental aerodynamic coefficients of a closed-box deck;

Case c) same as Case b) with the addition of the lateral motion to a 3DOF case;

In this paper, selected key results of Step 1.1a-c are presented.

### 2.2 Input for the analysis Step1.1a-c

#### 2.2.1 Structural data

Structural input data of the sectional model are reported in Table 1.

Table 1. Sectional model data

Quantity	Description	Value
$m_L$ [kg/m]	Mass per unit length	22740
$J_L$ [kgm <sup>2</sup> /m]	Moment of Inertia per unit length	$2.47 \times 10^6$
$B$ [m]	Deck chord	31
$\xi$ [-]	Damping ratio	0.003
$f_y$ [Hz]	Lateral natural frequency	0.052
$f_z$ [Hz]	Vertical natural frequency	0.10
$f_\theta$ [Hz]	Torsional natural frequency	0.278

#### 2.2.2 Turbulent wind

The characteristics of the simulated wind (along wind component  $u$  and vertical component  $w$ ) are reported in Table 2. From these characteristics ten time series of 10-min turbulent wind were generated using a spectral approach for time domain simulations (e.g. [24][25]): as an example, Figure 1 shows a time history of  $w$  at 60 m/s of mean wind speed ( $\Delta t = 0.05$  s).

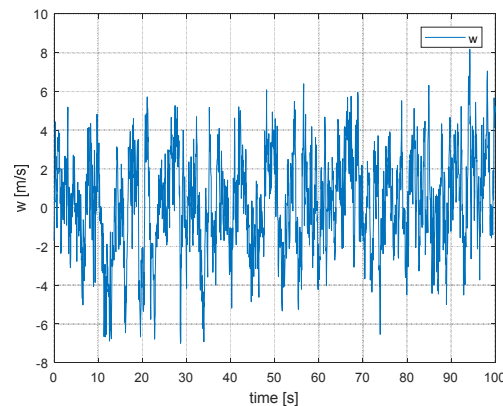


Figure 1. Example of simulated time history of  $w$  at 60 m/s of mean wind speed

The employed wind generator was selected for convenience whereas the investigation of wind and wind field generation problem is beyond the scope of this study.

Table 2. Incoming wind characteristics

<b>Wind speeds</b>	$U = 15, 30, 45, 60, 75$ m/s
<b>Air density</b>	$\rho = 1.22$ kg/m <sup>3</sup>
<b>Turbulence intensity</b>	$I_u = \frac{\sigma_u}{U} = 0.10$ ; $I_w = \frac{\sigma_w}{U} = 0.05$
<b>Integral length scale</b>	$^xL_u = 200$ m; $^xL_w = 20$ m
<b><math>u</math> and <math>w</math> spectra</b>	$\frac{f \cdot S_u(f)}{\sigma_u^2} = \frac{4 \left( \frac{f \cdot xL_u}{U} \right)}{\left[ 1 + 70.8 \left( \frac{f \cdot xL_u}{U} \right)^2 \right]^{5/6}}$ $\frac{f \cdot S_w(f)}{\sigma_w^2} = \frac{4 \left( \frac{f \cdot xL_w}{U} \right) \left( 1 + 755.2 \left( \frac{f \cdot xL_w}{U} \right)^2 \right)}{\left[ 1 + 283.2 \left( \frac{f \cdot xL_w}{U} \right)^2 \right]^{11/6}}$ $S_{uw}(f) = 0$

### 2.2.3 Aerodynamic forces

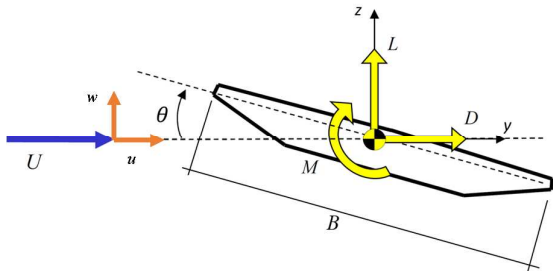


Figure 2. Sign conventions

With a reference to the conventions reported in Figure 2, the aeroelastic forces per unit length are defined through the flutter derivatives reported below. The scientific terminology by Politecnico di Milano is adopted for convenience whereas conversions to the classic Scanlan and Davenport formulae have been undertaken internally by the workgroup and will be included in the final report of this study.

$$D_{se} = \frac{1}{2} \rho U^2 B \begin{pmatrix} -p_1^* \frac{\dot{z}}{U} - p_2^* \frac{B\dot{\theta}}{U} + p_3^* \theta + \dots \\ \frac{2\pi^3}{V^{*2}} p_4^* \frac{z}{B} - p_5^* \frac{\dot{y}}{U} + \frac{2\pi^3}{V^{*2}} p_6^* \frac{y}{B} \end{pmatrix} \quad (1)$$

$$L_{se} = \frac{1}{2} \rho U^2 B \begin{pmatrix} -h_1^* \frac{\dot{z}}{U} - h_2^* \frac{B\dot{\theta}}{U} + h_3^* \theta + \dots \\ \frac{2\pi^3}{V^{*2}} h_4^* \frac{z}{B} - h_5^* \frac{\dot{y}}{U} + \frac{2\pi^3}{V^{*2}} h_6^* \frac{y}{B} \end{pmatrix} \quad (2)$$

$$M_{se} = \frac{1}{2} \rho U^2 B^2 \begin{pmatrix} -a_1^* \frac{\dot{z}}{U} - a_2^* \frac{B\dot{\theta}}{U} + a_3^* \theta + \dots \\ \frac{2\pi^3}{V^{*2}} a_4^* \frac{z}{B} - a_5^* \frac{\dot{y}}{U} + \frac{2\pi^3}{V^{*2}} a_6^* \frac{y}{B} \end{pmatrix} \quad (3)$$

In the aeroelastic forces per unit length defined above,  $h_i^*$  are the flutter derivatives for lift force;  $a_i^*$  are the flutter derivatives for the moment;  $p_i^*$  are the flutter derivatives for drag force;  $V^* = U/(fB)$  is the reduced velocity, being  $f$  the vibration frequency.

For Case a), the flat plate flutter derivatives values are used (from Theodorsen function), while, for

Case c), the experimental flutter derivatives of the Storebaelt bridge deck measured in wind tunnel are used. Coefficients are reported in Figures 3–4, only for 0 deg mean angle of attack.

The buffeting forces in both cases a) and c) are defined as:

$$\begin{Bmatrix} D_{buff} \\ L_{buff} \\ M_{buff} \end{Bmatrix} = \frac{1}{2} \rho U^2 B \begin{bmatrix} \chi_{Du}^* & \chi_{Dw}^* \\ \chi_{Lu}^* & \chi_{Lw}^* \\ B\chi_{Mu}^* & B\chi_{Mw}^* \end{bmatrix} \begin{Bmatrix} \frac{u}{U} \\ \frac{w}{U} \end{Bmatrix} \quad (4)$$

Where  $u$  and  $w$  are the horizontal and vertical incoming turbulence components and the  $\chi^*$  are called admittance functions and depend upon the  $V^*$ . The  $\chi^*$  are defined using the quasi-steady values weighed by the Davenport function  $A(V^*)$  as:

$$\begin{aligned} \chi_{Du}^* &= 2C_D A(V^*) = 0.154 A(V^*) \\ \chi_{Lu}^* &= 2C_L A(V^*) = 0.134 A(V^*) \\ \chi_{Mu}^* &= 2C_M A(V^*) = 0.056 A(V^*) \\ \chi_{Dw}^* &= (K_D - C_L) A(V^*) = 0.203 A(V^*) \\ \chi_{Lw}^* &= (K_L + C_D) A(V^*) = 4.447 A(V^*) \\ \chi_{Mw}^* &= K_M A(V^*) = 1.17 A(V^*) \end{aligned} \quad (5)$$

where  $A(V^*)$  is a real weighing function in reduced velocity:

$$A(V^*) = \frac{2}{(7/V^*)^2} (7/V^* - 1 + e^{-7/V^*}) \quad (6)$$

The numerical values in Eq.(5) refer to Case c), while for Case a), the flat plate,  $K_L = 2\pi$ ,  $K_M = \pi/2$ ,  $K_D = 0$ , and  $C_D = C_L = C_M = 0$ .

### 2.3 Output for the analysis for Step1.1a-c

The following results are compared for both Cases a) and c):

1. Flutter stability:
  - a. Critical flutter speed;
  - b. frequencies and damping as a function of mean wind speed.
2. Buffeting response in turbulent flow:

- a. standard deviation of displacement as a function of mean wind speed;
- b. peak displacements as a function of mean wind speed; and
- c. comparison of PSD.

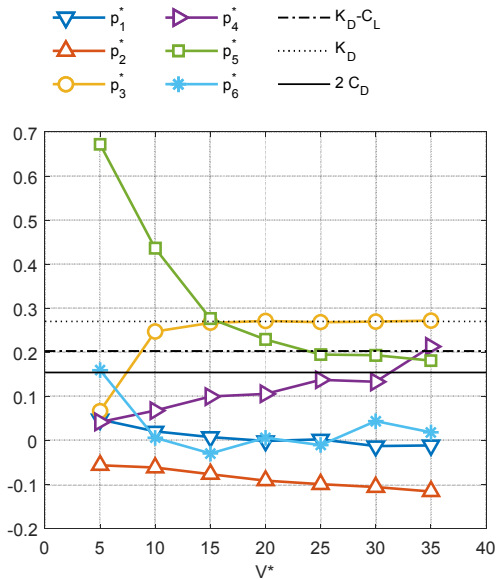


Figure 3. Drag derivatives: Storebaelt  $p^*$  values as a function of  $V^*$ , and QST coefficients

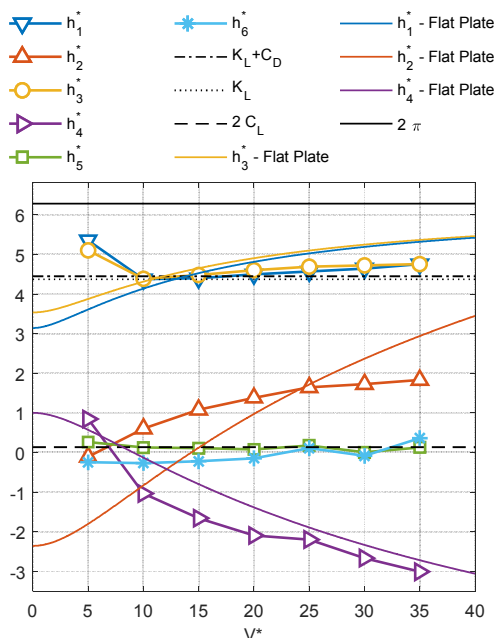


Figure 4. Lift derivatives Storebaelt and flat-plate  $h^*$  values as a function of  $V^*$ , and QST coefficients

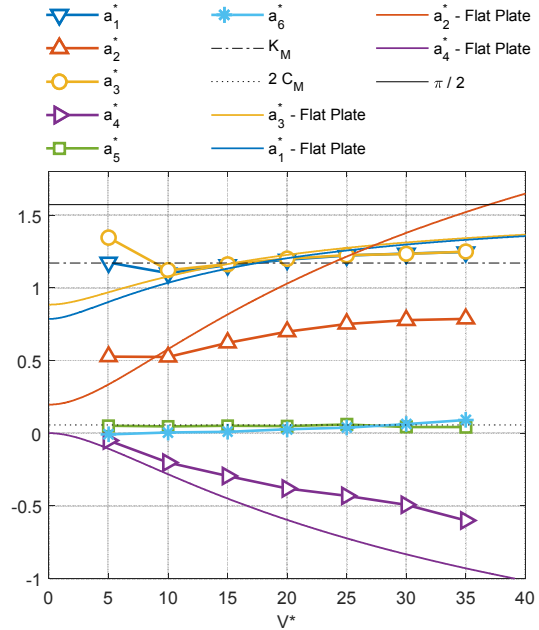


Figure 5. Moment derivatives Storebaelt and flat-plate  $a^*$  values as a function of  $V^*$ , and QST coefficients

### 3 Results

#### 3.1 Stability in laminar flow Step1.1a

Figure 6 shows a plot of the flutter critical speeds computed by the different methods and software programs owned by the TG members. Each contribution is defined anonymously by a number. To establish the reference result, the following procedure is applied:

1. The mean  $\mu^*$  and the standard deviation  $\sigma^*$  of all data is computed.
2. The data outside  $\mu^* \pm \sigma^*$  are considered outlier data.
3. The reference mean  $\mu$  and standard deviation  $\sigma$  are computed excluding the outlier data
4. Results within  $\mu \pm \sigma$  are considered valid

Both statistics are shown in Figure 6, to better understand this procedure: in the following results

only  $\mu \pm \sigma$  are shown. The reference is defined as  $\mu = 77.46$  m/s and  $\sigma = 0.095$  m/s.

The natural frequencies and the damping ratios of the system as function of the mean wind speed were computed and, as an example, the trends of frequency and damping of the unstable mode are reported in Figure 7 and Figure 8.

In this last case the lines  $\mu \pm \sigma$  are not reported for a better understanding of the plot. Most of the differences are close to the flutter critical wind speed. In any case, it is evident that majority of the results are quite similar.

### 3.2 Buffeting response Step1.1a

The root mean square (RMS) of the vertical ( $z$ ) and torsional displacement ( $\theta$ ) versus the wind mean speed are presented in Figure 9 and Figure 10. The torsional values are expressed in equivalent displacement of the deck leading edge according to:  $z_{eq} = \frac{B}{2}\theta$ , being  $B$  the deck chord. Frequency domain results (FD) are compared to time domain results (TD), where the plotted points are the average of the values of the results obtained with ten time histories of wind speed.

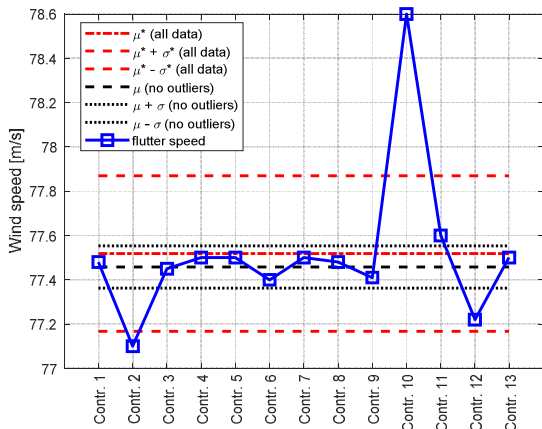


Figure 6. Flutter critical wind speed results from different programs of the TG. Red lines: statistical values using all data; Black lines: statistical values excluding outlier data

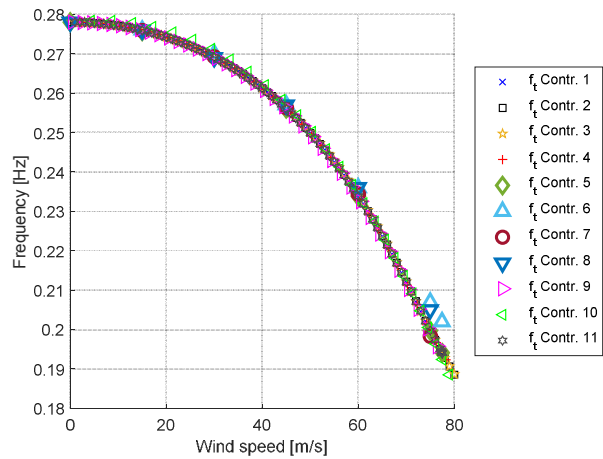


Figure 7. Frequency of the unstable mode as function of mean wind speed

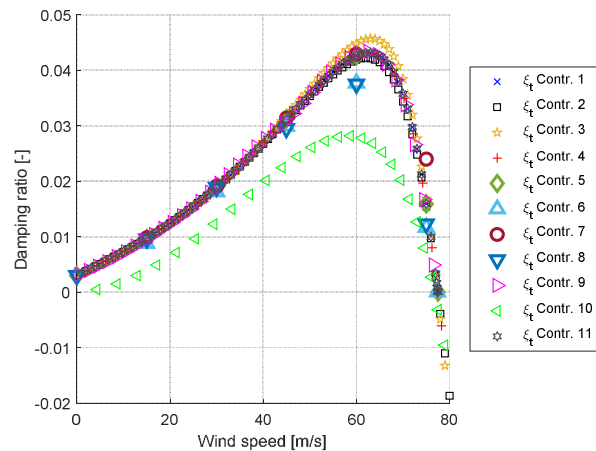


Figure 8. Damping ratio of the unstable mode as function of mean wind speed

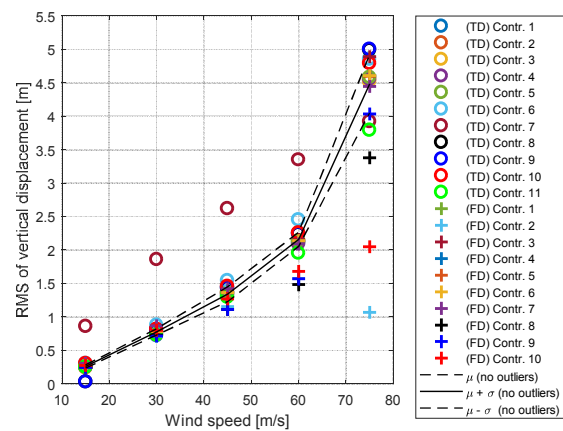


Figure 9. RMS of vertical displacement versus mean wind speed. Black lines: statistical values excluding outlier data

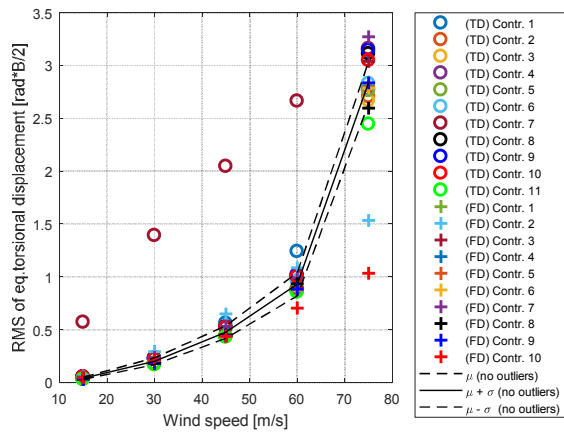


Figure 10. RMS of equivalent torsional displacement versus mean wind speed. Black lines: statistical values excluding outlier data

### 3.3 Stability in laminar flow Step1.1c

Figure 11 shows a plot of the flutter critical speeds predicted by different TG members for Step 1.1c. Both statistics are shown in Figure 11, where the reference statistics is  $\mu = 72.14$  m/s and  $\sigma = 0.275$  m/s.

The natural frequencies and damping ratios of the 3DOF system as a function of the mean wind speed are computed. In Figure 12 and Figure 13 below, the frequencies and damping ratios of all solutions are displayed, where the line  $\mu \pm \sigma$  is not reported for simplicity of the plot.

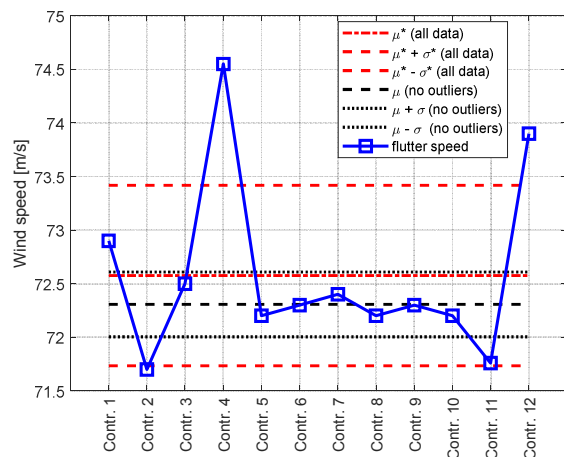


Figure 11 Flutter critical wind speed results from different programs of the TG. Red lines: statistical values using all data; Black lines: statistical values excluding outlier data

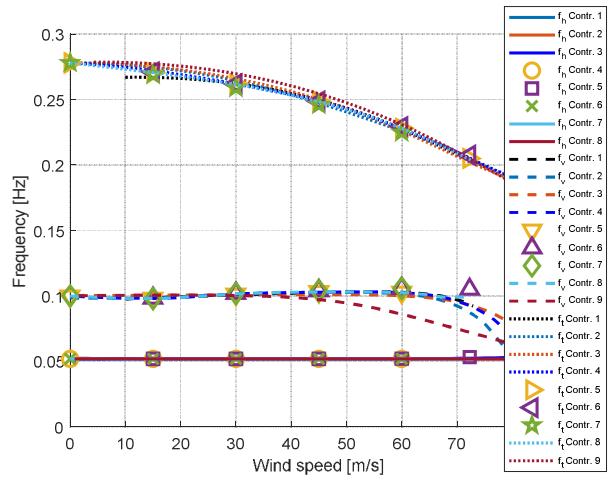


Figure 12. Frequency of the 3 DOF system as function of mean wind speed

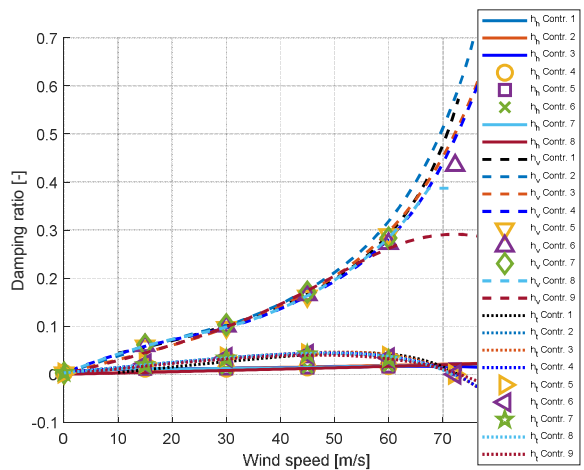


Figure 13. Damping ratio of the 3 DOF system as function of mean wind speed

### 3.4 Buffeting response Step1.1c

The root mean square (RMS) of the lateral ( $y$ ), vertical ( $z$ ) and torsional displacement ( $z_{eq}$ ) versus the wind mean speed are presented in Figure 14, Figure 15 and in Figure 16. The torsional values are expressed in equivalent displacement of the deck leading edge. Frequency domain results (FD) are compared to time domain results (TD), where the plotted points are the average of the values of the ten time histories. Each contribution by the TG members is defined anonymously as before.

Figure 17 and Figure 18 display the comparison of the power spectral density (PSD) in frequency and

time domain, in terms of vertical ( $z$ ) and torsional equivalent displacement ( $z_{eq}$ ). The value of RMS ( $RMS_z$  and  $RMS_{z_{eq}}$ ) computed by integration of the PSD values are reported in the legend. In this case just the line  $\mu$  is reported for a better understanding of the plot. The reference mean  $\mu$  is computed excluding the outlier data and considering the results only in frequency domain.

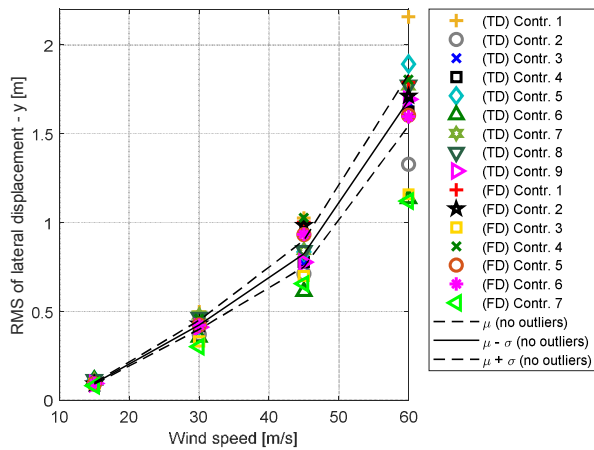


Figure 14. RMS of lateral displacement versus mean wind speed

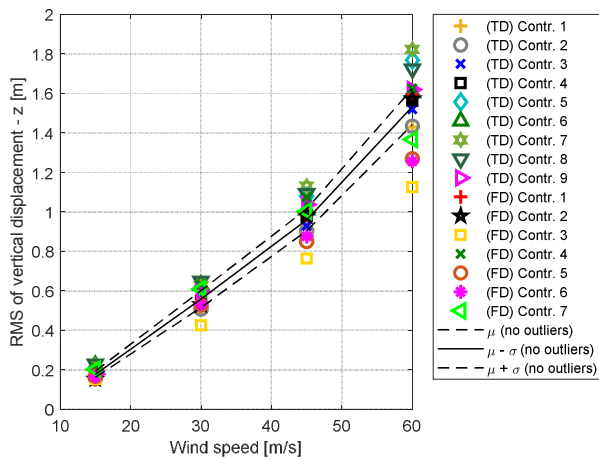


Figure 15. RMS of vertical displacement versus mean wind speed

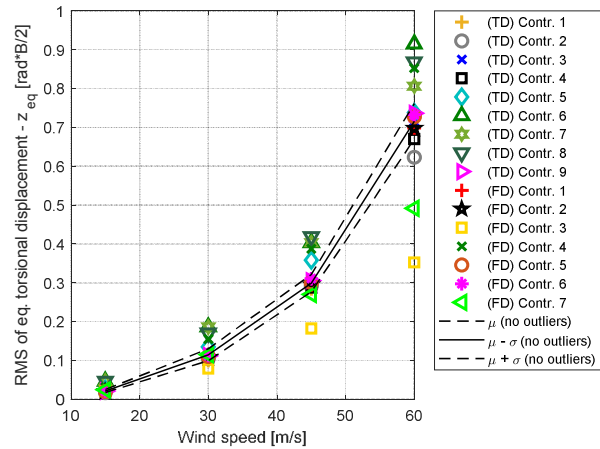


Figure 16. RMS of equivalent torsional displacement versus mean wind speed

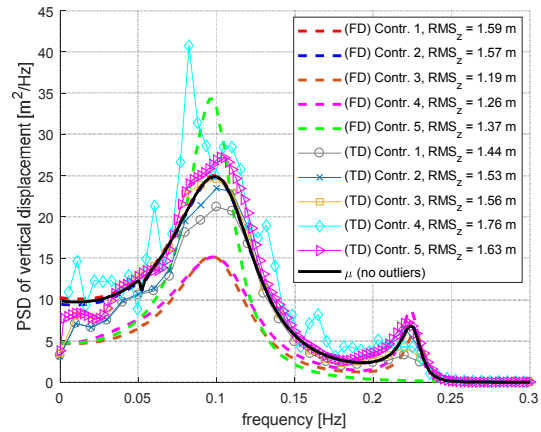


Figure 17. PSD of vertical displacement, 60 m/s wind mean speed

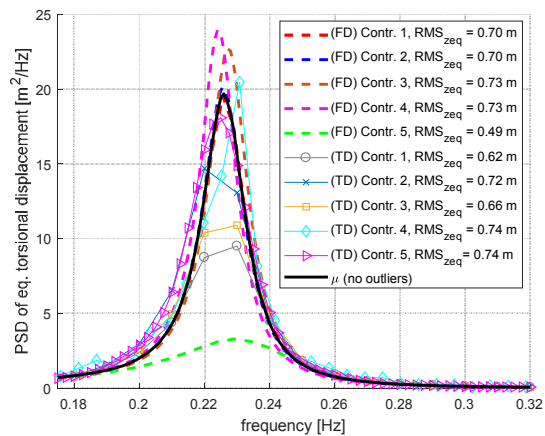


Figure 18. PSD of equivalent torsional displacement, 60 m/s wind mean speed

## 4 Conclusions

This paper presents first results of Step 1.1 of the benchmark study. Even if this task involved the simplest possible 1-strip, 3DOF model, noticeable differences arose during the result comparisons.

Similar critical flutter velocities were predicted, however the trend of the eigenvalues (frequency and damping) as a function of the wind speed showed in some cases significant differences. Even larger discrepancies were observed using the experimental aerodynamic coefficients for the 3DOF case including the lateral motion for Step 1.1c, due likely to interpolation/extrapolation of experimental data. In Figure 11, for example, the standard deviation  $\sigma$  computed excluding the outlier data is higher.

Buffeting response was computed in time and frequency domain. Concerning Step 1.1a, it is surprising to find a dispersion of results in frequency domain as the flutter derivatives are defined by the Theodorsen function and therefore continuous over the spectrum of frequencies. Considering time domain analysis which is somewhat newer and more complex method to compute the bridge response to the turbulent wind where each participant has its own software, the larger dispersion of results has been expected.

The response predictions of the 3DOF case presents more difficulties due to the interpolation of experimental flutter derivatives both in terms of aeroelastic stability and buffeting response.

Removing the outliers, and given the majority of the remaining predictions are reasonably close, the results within the  $\mu \pm \sigma$  interval appear reasonable. This task group therefore believes these can be used as a reference for the validation of methodologies and software programs pursuing the ability to predict critical flutter speed and buffeting response of long-span bridges for the 3DOF case considered.

## 5 References

- [1] Bucher CG, and Lin YK. Stochastic stability of bridges considering coupled modes. *Journal of Engineering Mechanics*. 1988; **114**(12): 2055-2071.
- [2] Chen X, Matsumoto M, and Kareem A. Time domain flutter and buffeting response analysis of bridges. *Journal of Engineering Mechanics*. 2000; **126**(1):7-16.
- [3] Kavrakov I, Morgenthal G. A comparative assessment of aerodynamic models for buffeting and flutter of long-span bridges. *Engineering*. 2017; **3**:823-838
- [4] Garrick IE. On some reciprocal relations in the theory of nonstationary flows. Technical report, NACA, 1938.
- [5] Jain A, Jones NP, and Scanlan RH. Coupled Flutter and Buffeting Analysis of Long-Span Bridges. *Journal of Structural Engineering*. 1996; **122**(7):716-725.
- [6] Oiseth O, Ronnquist A, and Sigbjornsson R. Simplified prediction of wind-induced response and stability limit of slender long-span suspension bridges, based on modified quasi-steady theory: A case study. *Journal of Wind Engineering and Industrial Aerodynamics*. 2010; **98**(12):730-741.
- [7] Oiseth O, Ronnquist A, and Sigbjornsson R. Time domain modeling of self-excited aerodynamic forces for cable-supported bridges: A comparative study. *Computers & Structures*. 2011; **89**(13-14):1306-1322.
- [8] Oiseth O, Ronnquist A, and Sigbjornsson R. Finite element formulation of the self-excited forces for time-domain assessment of wind-induced dynamic response and flutter stability limit of cable-supported bridges. *Finite Elements in Analysis and Design*. 2012; **50**:173-183.
- [9] Oiseth O, and Sigbjornsson R. An alternative analytical approach to prediction of flutter stability limits of cable supported bridges. *Journal of Sound and Vibration*. 2011; **330**(12):2784-2800.
- [10] Shinozuka M, and Jan CM. Digital simulation of random processes and its applications. *Journal of Sound and Vibration*. 1972; **25**(1):111-128.
- [11] Shinozuka M. Monte Carlo solution of structural dynamics. *Computers and Structures*. 1972; **2**(5-6):855-874.

- [12] Stoyanoff S. A unified approach for 3D stability and time domain response analysis with application of quasi steady theory, *Journal of Wind Engineering and Industrial Aerodynamics*. 2001; **89**:1591–1606.
- [13] Stoyanoff S, and Dallaire PO. A direct method for calculation of wind loads on long- span bridges. *12th Americas Conference on Wind Engineering (12ACWE)*, Seattle, Washington, USA, June 16-20, 2013.
- [14] Stoyanoff S. Wind Induced Vibrations of Cable-Stayed Bridges, *Ph.D. Thesis*, Graduate School of Engineering, Kyoto University, Japan, 1993.
- [15] Park J, Jung K, Hong YH, Kim HK, and Lee HS. Exact Enforcement of the Causality Condition on the Aerodynamic Impulse Response Function Using a Truncated Fourier Series. *Journal of Engineering Mechanics*. 2014; **140**(5).
- [16] Jung K, Kim HK, and Lee HS. New Unified Approach for Aeroelastic Analyses Using Approximate Transfer Functions of Aerodynamic Forces. *Journal of Engineering Mechanics*. 2013; **140**(4).
- [17] Jung K, Kim HK, and Lee HS. Evaluation of impulse response functions for convolution integrals of aerodynamic forces by optimization with a penalty function. *Journal of Engineering Mechanics*. 2011; **138**(5), 519-529.
- [18] Strømmen EN, Theory of Bridge Aerodynamics.
- [19] Matsumoto M, Okubo K, Ito Y, Matsumiya H, and Kim G. The complex branch characteristics of coupled flutter. *Journal of Wind Engineering and Industrial Aerodynamics*. 2011; **96**(10):1843-1855.
- [20] Høgsberg JR, Krabbenhøft J, and Krenk S. State space representation of bridge deck aeroelasticity, *13th Nordic Seminar on Computational Mechanics*, October 20-21, Oslo, Norway, 2000.
- [21] Argentini T, Pagani A, Rocchi D, and Zasso A. Monte Carlo analysis of total damping and flutter speed of a long span bridge: Effects of structural and aerodynamic uncertainties. *Journal of Wind Engineering and Industrial Aerodynamics*. 2014; **128**:90-104
- [22] Diana G, Rocchi D, and Argentini T. An experimental validation of a band superposition model of the aerodynamic forces acting on multi-box deck sections. *Journal of Wind Engineering & Industrial Aerodynamics*. 2013; **113**:40-58
- [23] Diana G, Rocchi D, and Argentini T. Buffeting response of long span bridges: numerical-experimental validation of fluid-structure interaction models *IABSE Conference - Structural Engineering: Providing Solutions to Global Challenges*, 2015
- [24] Ding Q, Zhu L, and Xiang H. Simulation of stationary Gaussian stochastic wind velocity field. *Wind and Structures, An International Journal*, 2006; **9**:231-243.
- [25] Deodatis G. Simulation of ergodic multivariate stochastic processes. *Journal of Engineering Mechanics*. 1996; **122**:778-78



40th IABSE Symposium, 19-21 September 2018, Nantes, France.  
Tomorrow's Megastructures

- 1
- 2
- 3
- 4
- 5
- 6
- 7
- 8
- 9
- 10
- 11
- 12
- 13
- 14
- 15
- 16
- 17
- 18
- 19
- 20
- 21
- 22
- 23
- 24
- 25
- 26
- 27
- 28
- 29
- 30
- 31
- 32
- 33
- 34
- 35
- 36
- 37
- 38
- 39
- 40
- 41
- 42
- 43
- 44
- 45
- 46
- 47
- 48
- 49
- 50
- 51
- 52
- 53
- 54
- 55
- 56
- 57
- 58
- 59
- 60